Analytical and numerical analyses of the load-bearing capacity of retaining walls laterally supported at both ends

Sylvain Plumey[1,2,*,†], Aurelio Muttoni[1,2], Laurent Vulliet[1,3] and Vincent Labiouse[1,4]

[1]*Ecole Polytechnique Fédérale de Lausanne, Lausanne, Switzerland*
[2]*Structural Concrete Laboratory, Lausanne, Switzerland*
[3]*Soil Mechanics Laboratory, Lausanne, Switzerland*
[4]*Rock Mechanics Laboratory, Lausanne, Switzerland*

SUMMARY

This paper investigates the load-bearing capacity of a perfectly smooth retaining wall laterally supported at both ends assuming that the wall fails by the development of three plastic hinges. The study considers the case of a cohesionless elastic–perfectly plastic backfill with a Mohr–Coulomb yield criterion and an associative flow rule in drained conditions. A kinematically admissible soil–structure failure mechanism is proposed and compared with the conventional solutions and with results from a numerical finite element modelling. The study shows that the proposed solution and the numerical solution are in good agreement. These solutions are found to be much more favourable for the wall than the conventional solutions. Copyright © 2010 John Wiley & Sons, Ltd.

1. INTRODUCTION

The lateral earth pressure acting on a retaining structure depends on the deformation of the structure and of the surrounding soil. It is thus a function of the properties of the soil and of the structure, as well as of the support conditions of the structure and of its construction process. The earth pressure behind a rigid cantilever wall is known to be very different from the earth pressure behind a flexible anchored sheet pile wall [1]. Similarly, for a given structure, the earth pressure and its distribution along the wall under service conditions, characterized by small deformations, considerably change when the structure gets close to failure, which is usually characterized by important deformations.

The collapse of a retaining structure can occur according to different failure mechanisms, which must all be considered in design, as mentioned by the recent codes of practice [2, 3]. In the general case, the collapse is either due to the failure of the soil, the structure having a rigid body motion, or due to a combined failure of the soil and of the structure. In the latter case, the structure generally controls the behaviour of the soil because its failure mechanism also defines the failure pattern in the surrounding soil and controls its development. In such cases, a suitable evaluation of the earth pressure at failure must thus be based on a correct consideration of the failure mechanism. A corollary is that the design of such structures at ultimate limit state must be based on a realistic

*Correspondence to: Sylvain Plumey, Ecole Polytechnique Fédérale de Lausanne, Lausanne, Switzerland.
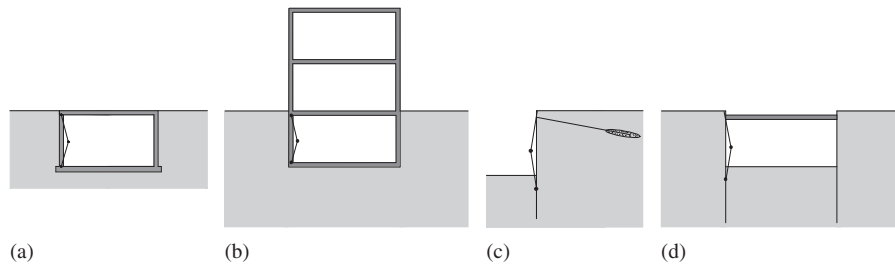†E-mail: s.plumey@buchs-plumey.ch

Figure 1. Situations where the studied failure mechanism may govern the behaviour: (a) frame-shaped cut-and-cover tunnel (construction stage); (b) building basement; (c) anchored wall; and (d) braced cut.

earth pressure, accounting for the actual failure mechanism. This conclusion is at the base of Brinch Hansen's work on the calculation of earth pressure [4].

If both the soil and the structure are assumed to be perfectly plastic materials with associative flow rules, the behaviour of such structures can be investigated by means of the theory of plasticity [5–7]. Upper-bound solutions can then be found based on assumed failure mechanisms, which must be kinematically admissible for the soil and for the structure. This paper presents one upper-bound solution for the load-bearing capacity of a retaining wall laterally supported at both extremities, assuming a bending failure of the wall. This paper is limited to soils with zero cohesion. This assumption, which is acceptable for structures in contact with backfill, simplifies the mathematical development of the proposed solution. The solution could, however, be generalized to soils with cohesion following a similar procedure. Developed initially for frame-shaped cut-and-cover tunnels, this solution can also be applied to cases where a bending failure may be considered, such as basement walls, anchored walls or braced cuts (see Figure 1). Comparisons with the results obtained with the finite element method (FEM) and with the conventional solutions are also discussed.

2. PROBLEM STATEMENT AND ASSUMPTIONS

The wall considered in this paper, presented in Figure 2(a), is a lateral wall of a frame-shaped tunnel built by the cut-and-cover method. The investigated situation is obtained after the backfill reaches the top of the wall. A uniformly distributed load q is applied on the soil-free surface. The lower and upper ends of the wall are laterally supported. The capacity of the support to transmit bending moments can also be appreciated. This capacity is governed by the bearing capacity of the foundation and of the top slab for the lower and upper extremities, respectively. The situation is assumed to be in plane strain state.

Such structures are usually made in reinforced concrete. If brittle failures (shear, anchorage failures) are avoided by suitable design measures, the failure is expected to occur in bending after the development of plastic hinges at both extremities (if bending is restrained) and in the central region of the wall. The location of the latter plastic hinge is, however, not known *a priori*.

The soil is assumed to be rigid perfectly plastic material with a Mohr–Coulomb yield criterion and with negligible cohesion. Its plastic flow rule is assumed to be associative, so that the upper-bound theorem of limit analysis is applicable [5, 7]. In a Mohr diagram showing simultaneously the stresses and the incremental plastic strains, the plastic incremental strain, or strain-rate, is then perpendicular to the yield criterion (see Figure 3(b)). Drained conditions with large permeability are assumed, so that transient effects linked to the hydro-mechanical coupling can be neglected.

The behaviour of the reinforced concrete wall is assumed to be rigid perfectly plastic. The flexural behaviour is thus defined by its flexural strength M_R, assumed to be constant along the wall, and is represented schematically in Figure 3(a). The flexural strengths of the lower and upper supports are defined by $\eta_l M_R$ and $\eta_u M_R$, respectively. The wall thickness is neglected in the following analysis.
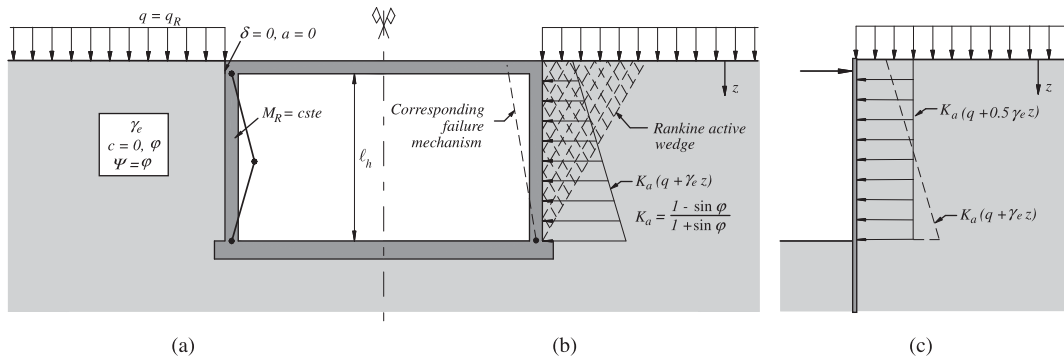
Figure 2. Investigated case: (a) failure mechanism of the wall and properties; (b) earth pressures along the wall assuming a Rankine active stress state in the soil; and (c) earth pressures in the case of braced cuts according to Terzaghi and Peck [1].
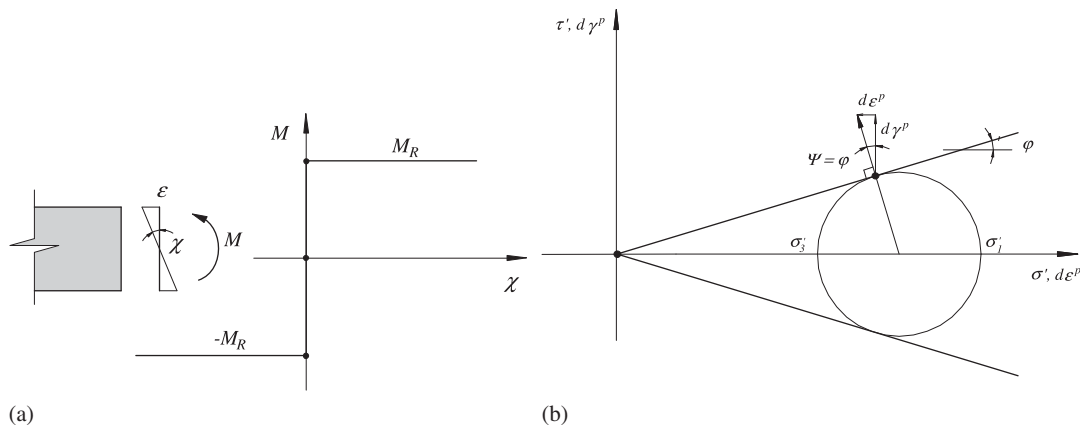

Figure 3. Assumed behaviours: (a) flexural behaviour of the wall and (b) yield criterion and flow rule of the soil.

The interface between the soil and the structure is assumed to be perfectly smooth, meaning that free slip is permitted along the wall.

The stated problem is to determine the ultimate load q_R supported by a wall with flexural strength M_R, support conditions η_l and η_u and height ℓ_h retaining a soil characterized by a unit weight γ_e, a friction angle φ and zero cohesion.

3. CURRENT PRACTICE AND THEORETICAL SOLUTIONS

When the top end of the wall is free, i.e. in the case of a cantilever wall, the exact solution corresponds to the linear active earth pressure distribution first formulated by Rankine [8]. This mechanism is kinematically incompatible with the top end of the braced wall (see Figure 2(b)). As this stress state does not violate the yield criterion anywhere in the soil and is statically admissible, this assumption, however, leads to a safe design if the wall is ductile (lower-bound theorem of limit analysis) and is accepted for the design of cut-and-cover tunnels [9]. Nevertheless, multi-popped walls of cuts are generally designed in practice assuming a constant averaged earth pressure along the wall whose intensity is generally obtained by redistributing a Rankine active earth pressure [1, 10–12]. The reason of redistributing the active Rankine earth pressure was first motivated by field measurements, which indicated important differences between measured and theoretical forces in the struts, with increased forces in the upper struts [13].

These measurements clearly reflect the behaviour of such structures under service conditions and distinction should here be made with the ultimate limit state. These redistributed earth pressures were also a consequence of the need to have a safe estimate of the forces in the struts, whose resistance is generally limited by buckling. It should be emphasized that limit analysis is not applicable to cases governed by structural instabilities, such as geometric bifurcations or brittle behaviours.

Relatively little research effort has been carried out on theoretical solutions of the stated problem in spite of its significant practical implications, perhaps because of the recent advent of the finite element method, which offers a powerful tool to designers.

Brinch Hansen proposed a systematic method to determine the earth pressure acting on retaining structures that explicitly consider the failure mechanism of the structure [4]. However, the method is based on some simplifications and the obtained solutions are neither upper bounds nor lower bounds. One limitation is due to the use of circular failure lines, which are not kinematically admissible for soils with non-zero friction angle. A simplified method of Brinch Hansen's original method applied to a retaining wall failing in bending ('three hinges' pattern) can also be found in [14].

More research effort was put in a similar case, which is of greater interest for anchored sheet pile walls. A retaining wall rotating about its top was investigated by Steenfelt [15], who proposed a rupture figure, which suggests the development of a so-called plasticized trumpet zone in the soil. This was indeed confirmed by finite element analyses made by Mortensen and Steenfelt [16]. This study also showed that logarithmic spiral failure lines were able to reproduce reasonably well the failure mechanism obtained with the numerical model.

4. PROPOSED MECHANISM

4.1. Kinematics

The proposed failure mechanism is shown in Figure 4 with a distinction being made between the structure and the soil. It is fully described by the two geometrical parameters ξ and x, defined in Figure 4 and described below, and by the velocity (or incremental plastic strain) of the plastic hinge located in the central region of the wall v_{h0}.

4.1.1. Wall kinematics. The failure mechanism of the wall itself is only described by the parameter ξ, which defines the location of the plastic hinge in the central region of the wall (see Figure 4(a)). The structure is then composed of two parts delimited by the three plastic hinges (AE and AD), each one rotating about one support.

The rotations of the upper part of the wall about point E and of the lower part about point D are defined by the angular velocities given, respectively, by Equations (1) and (2):

$$\Omega_E = \frac{v_{h0}}{\xi \cdot \ell_h} = \frac{v_{h0}}{x \cdot \tan \theta_0} \tag{1}$$

$$\Omega_D = \frac{v_{h0}}{(1-\xi) \cdot \ell_h} = \frac{v_{h0}}{x \cdot (\tan \theta_f - \tan \theta_0)} \tag{2}$$

4.1.2. Soil kinematics. The failure mechanism in the soil is composed of two areas delimited by two logarithmic spirals having the same centre O (see Figure 4(b)). The first area ($ABEA$) located against the upper part of the wall is not plasticized. It is then subjected to a rigid body rotation, which must be compatible with the rotation of the upper part of the wall (AE). The centre of rotation O is aligned with the free surface because the horizontal component of the velocity of the soil in point E must be zero. Its position is then defined by the parameter x corresponding to the distance separating the centre of rotation O and the top of the wall E. The angular velocity of the region $ABEA$ is also given by Equation (1).
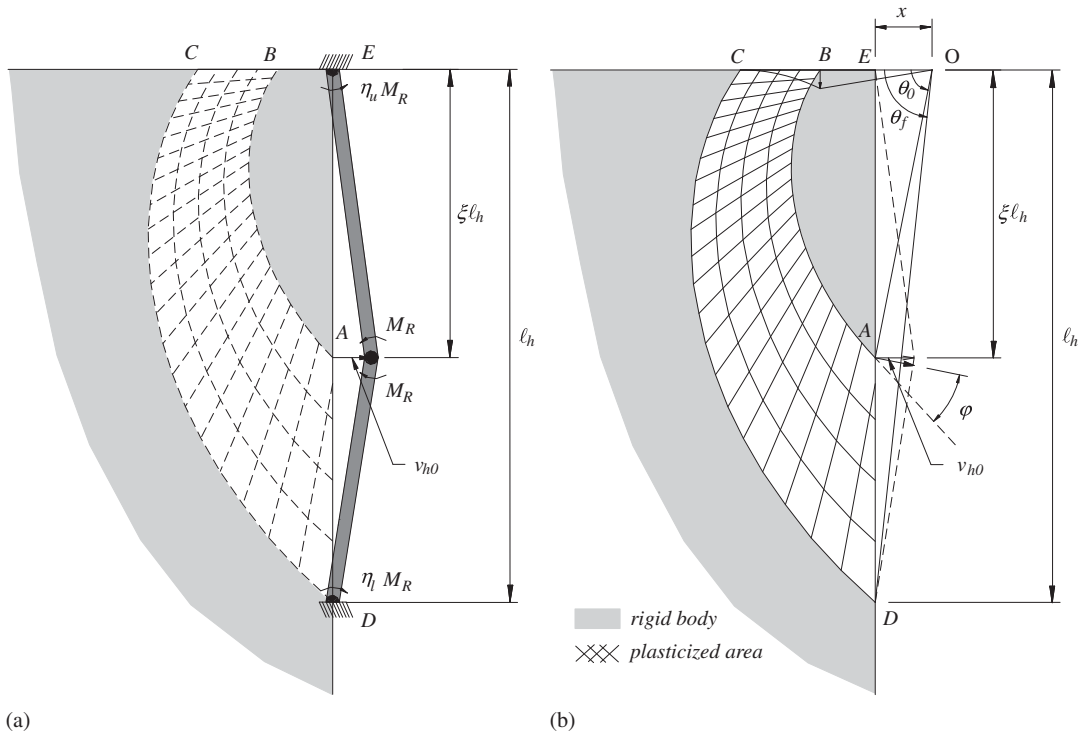
Figure 4. Proposed failure mechanism: (a) wall kinematics and (b) soil kinematics.

The second area (*ABCDA*) is plasticized and subjected to shear strains so that its movement is compatible with the rotation of the lower part of the wall (*AD*).

The kinematical compatibility at the interface between the soil and the structure is ensured by imposing that the horizontal component of the displacement of the soil along the structure is identical to the displacement of the structure. This condition enables to construct the velocity field in the area *ABCDA*.

The total velocity of the soil in point *A* is given by

$$v_{\theta_0} = \frac{v_{h0}}{\sin \theta_0} \tag{3}$$

The velocity of the soil along the lower part of the wall v_θ is given similarly using the angle $\theta \in [\theta_0; \theta_f]$ (defined in Figure 5(a)) and expressing the previously mentioned compatibility condition on the horizontal component of the velocity:

$$v_\theta = \frac{v_h}{\sin \theta} = \frac{v_{h0}}{\sin \theta} \cdot \frac{\tan \theta_f - \tan \theta}{\tan \theta_f - \tan \theta_0} \tag{4}$$

A relative slip between the soil and the wall is permitted according to the assumed mechanism. Thus, this solution is admissible only if the interface is perfectly smooth.

The area *ABCDA* can be seen as an infinity of concentric logarithmic spirals, each one being defined by one angle θ. The velocity $v_{\theta\alpha}$ of any point belonging to a given logarithmic spiral is expressed by Equation (5), where α defines the position of the point on the spiral (see Figure 5(a)).

$$v_{\theta\alpha} = v_\theta \cdot e^{\tan \varphi \cdot (\alpha - \theta)} \tag{5}$$

At any point in the area ABCDA, the velocity makes an angle φ with the logarithmic spirals, which is in agreement with the associative flow rule and thus ensures the kinematical admissibility of the velocity field [5, 6].
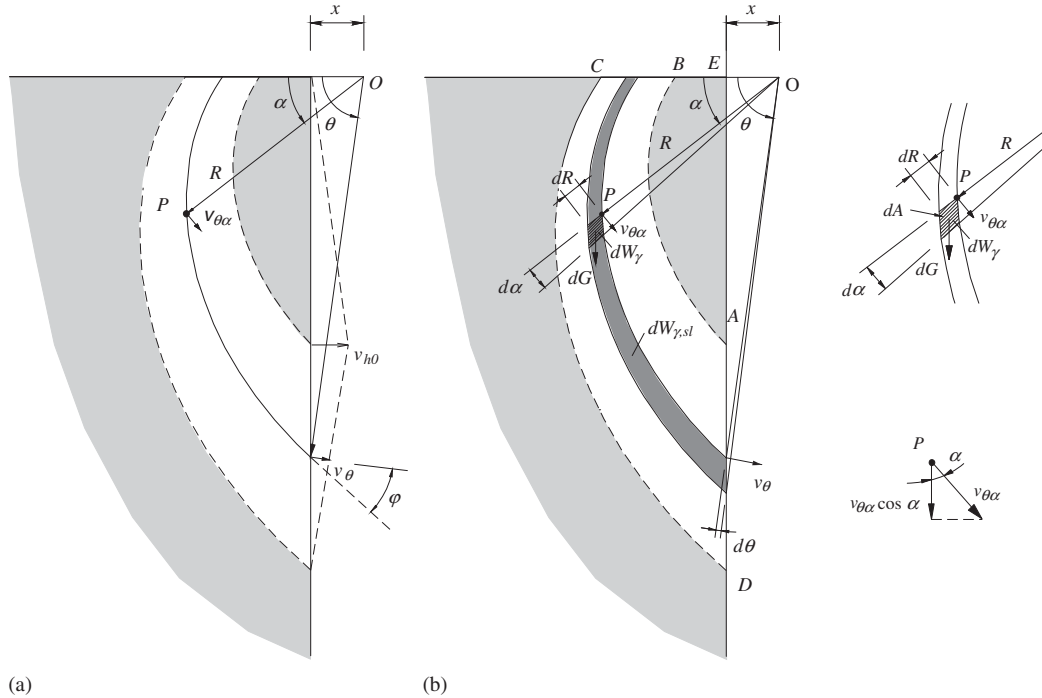
Figure 5. (a) Velocity of point P belonging to the area $ABCDA$ as a function of the parameters θ and α and (b) integration scheme for the work of region $ABCDA$.

4.1.3. Limit cases. The geometrical parameters are bound by the physical conditions $x \geqslant 0$ and $\xi \in [0; 1]$. Moreover, the couples (x, ξ) are restrained by the condition given by Equation (6), which expresses that the point B of the logarithmic spiral delimiting the rigid body $ABEA$ must be on the soil-free surface (limit case: $OB \equiv OE$).

$$\cos \theta_0 = e^{-\theta_0 \cdot \tan \varphi} \tag{6}$$

4.2. Principle of virtual works

For a given geometry, i.e. a wall of height ℓ_h and a couple of parameters $(\xi; x)$, the principle of the virtual works [7], recalled in Equation (7) where W_{ext} is the external work and D is the dissipation of energy produced under the assumed mechanism, can be used to determine an upper bound to the ultimate load q_R supported by a wall with flexural strength M_R and support conditions η_u and η_l retaining a soil characterized by a unit weight γ_e, a friction angle φ and zero cohesion.

$$W_{\text{ext}} + D = 0 \tag{7}$$

4.2.1. External work. The external work according to the proposed mechanism is produced by the load q and by the self weight of the soil.

Work of the self weight of the soil: The work W_γ produced by the self weight of the soil can be decomposed into the two contributions of the rigid body $ABEA$ and of the plasticized area $ABCDA$.

The work $W_{\gamma, ABEA}$ done by the area $ABEA$ can be rewritten as the work done by the region $OABO$ minus the work done by the region $OAEO$:

$$W_{\gamma, ABEA} = W_{\gamma, OABO} - W_{\gamma, OAEO} \tag{8}$$

The work of a rigid body delimited by a logarithmic spiral and two of its radii rotating about its centre O is given in [5]. Its application to the area $OABO$ rotating about O with a rotational velocity Ω_E leads to

$$W_{\gamma,OABO} = \gamma_e \cdot \left(\frac{x}{\cos\theta_0} e^{-\theta_0\tan\varphi} \right)^3 \cdot \Omega_E \cdot f_1(\theta_0) \tag{9}$$

with

$$f_1(\theta_0) = \frac{1}{27\tan^2\varphi} \cdot ((3\tan\varphi \cdot \cos\theta_0 + \sin\theta_0) \cdot e^{3\cdot\theta_0\tan\varphi} - 3\tan\varphi) \tag{10}$$

Introducing Equation (1) in Equation (10) gives the work done by the area $OABO$ expressed as a function of the velocity v_{h0}:

$$W_{\gamma,OABO} = \frac{1}{3}\gamma_e \cdot x^2 \cdot v_{h0} \cdot \frac{3\tan\varphi \cdot \cos\theta_0 + \sin\theta_0 - 3\tan\varphi \cdot e^{-3\theta_0\tan\varphi}}{\cos^2\theta_0 \cdot \sin\theta_0 \cdot 9\tan^2\varphi} \tag{11}$$

The work done by the triangular area $OAEO$ rotating about point O with a rotational velocity Ω_E is given by

$$W_{\gamma,OAEO} = \tfrac{1}{2}x^2 \cdot \tan\theta_0 \cdot \gamma_e \cdot \tfrac{2}{3} \cdot x \cdot \Omega_E = \tfrac{1}{3}\gamma_e \cdot x^2 \cdot v_{h0} \tag{12}$$

Inserting Equations (11) and (12) into Equation (8) gives the work done by the rigid body $ABEA$:

$$W_{\gamma,ABEA} = \frac{1}{3}\gamma_e \cdot x^2 \cdot v_{h0} \cdot \left(\frac{3\tan\varphi \cdot \cos\theta_0 + \sin\theta_0 - 3\tan\varphi \cdot e^{-3\theta_0\tan\varphi}}{\cos^2\theta_0 \cdot \sin\theta_0 \cdot 9\tan^2\varphi)} - 1 \right) \tag{13}$$

The work $W_{\gamma,ABCDA}$ done by the plastic zone $ABCDA$ can be obtained by following the integration procedure shown in Figure 5(b). The work done by an infinitesimal area dA delimited by two adjacent logarithmic spirals separated by dR and two radii separated by the angle $d\alpha$ is integrated over the full area $ABCDA$.

The infinitesimal area dA is given by

$$dA = R \cdot dR \cdot d\alpha \tag{14}$$

The radius R can be expressed as a function of the variables θ and α defining the position of the point P, which belongs to the infinitesimal area dA (see Figure 5(b)):

$$R(\theta,\alpha) = \frac{x \cdot e^{(\alpha-\theta)\cdot\tan\varphi}}{\cos\theta} \tag{15}$$

The infinitesimal area dA can be written as a function of θ:

$$dA = \frac{x^2}{\cos^2\theta} \cdot e^{2(\alpha-\theta)\cdot\tan\varphi} \cdot (\tan\theta - \tan\varphi) \cdot d\theta \cdot d\alpha \tag{16}$$

The infinitesimal work of the area dA is given by

$$dW_\gamma = \gamma_e \cdot dA \cdot v_{\theta\alpha} \cdot \cos\alpha \tag{17}$$

$v_{\theta\alpha}$ being the velocity of point P.

Introducing Equations (4), (5) and (16) into Equation (17) leads to

$$dW_\gamma = \gamma_e \cdot \frac{x^2}{\cos^2\theta} \cdot e^{3(\alpha-\theta)\cdot\tan\varphi}(\tan\theta - \tan\varphi) \cdot \frac{v_{h0}}{\sin\theta} \cdot \frac{\tan\theta_f - \tan\theta}{\tan\theta_f - \tan\theta_0} \cdot \cos\alpha \cdot d\theta \cdot d\alpha \tag{18}$$

The work of the area $ABCD$ is now obtained by integrating Equation (18) over the plastic domain with respect to the two variables θ and α:

$$W_{\gamma,ABCDA} = \int_{\theta=\theta_0}^{\theta_f} \int_{\alpha=0}^{\theta} dW_\gamma \tag{19}$$

The integration with respect to α leads to the work of an infinitesimal layer delimited by two adjacent logarithmic spirals $dW_{\gamma,\mathrm{sl}}$ (see Figure 5(b)):

$$dW_{\gamma,\mathrm{sl}} = \gamma_e \cdot \frac{x^2}{\cos^2\theta} \cdot (\tan\theta - \tan\varphi) \cdot \frac{v_{h0}}{\sin\theta} \cdot \frac{\tan\theta_\mathrm{f} - \tan\theta}{\tan\theta_\mathrm{f} - \tan\theta_0} \cdot \int_0^\theta e^{3(\alpha-\theta)\cdot\tan\varphi} \cdot \cos\alpha \cdot d\alpha \tag{20}$$

The solution to this integral, recalled by Chen in [5], is

$$dW_{\gamma,\mathrm{sl}} = \gamma_e \cdot \frac{x^2}{\cos^2\theta} \cdot (\tan\theta - \tan\varphi) \cdot \frac{v_{h0}}{\sin\theta} \cdot \frac{\tan\theta_\mathrm{f} - \tan\theta}{\tan\theta_\mathrm{f} - \tan\theta_0}$$

$$\cdot (3\tan\varphi \cdot \cos\theta + \sin\theta - 3\tan\varphi \cdot e^{-3\theta\cdot\tan\varphi}) \tag{21}$$

In light of Equation (21), the work of the area *ABCDA* can be rewritten as

$$W_{\gamma,ABCDA} = \int_{\theta=\theta_0}^{\theta_\mathrm{f}} dW_{\gamma,\mathrm{sl}} = \int_{\theta_0}^{\theta_\mathrm{f}} \gamma_e \cdot \frac{x^2}{\cos^2\theta} \cdot (\tan\theta - \tan\varphi) \cdot \frac{v_{h0}}{\sin\theta} \cdot \frac{\tan\theta_\mathrm{f} - \tan\theta}{\tan\theta_\mathrm{f} - \tan\theta_0}$$

$$\cdot (3\tan\varphi \cdot \cos\theta + \sin\theta - 3\tan\varphi \cdot e^{-3\theta\cdot\tan\varphi}) \cdot d\theta \tag{22}$$

The solution to this integral can be obtained numerically.

As the work done by the self weight of the soil (Equations (13) and (22)) is a function of the two geometrical parameters ξ and x, it can be expressed in the form as

$$W_\gamma = W_{\gamma,ABEA} + W_{\gamma,ABCDA} = v_{h0} \cdot \overline{W}_\gamma = v_{h0} \cdot f(\xi,x) \tag{23}$$
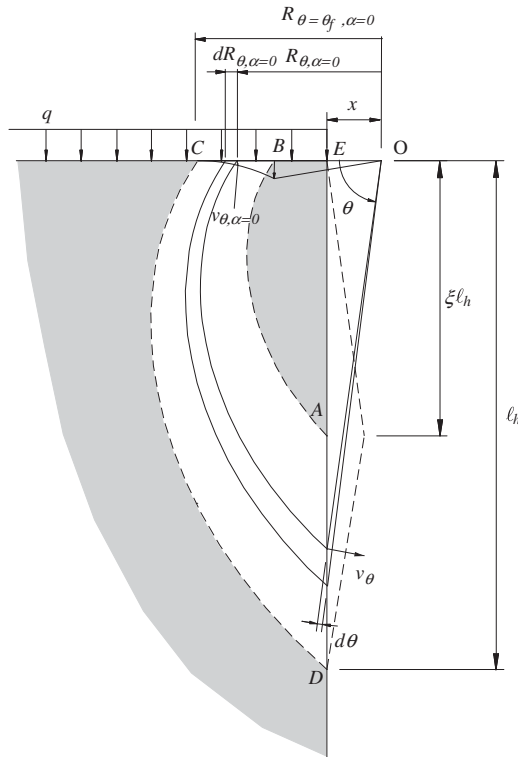

Figure 6. Integration scheme for the work of the load q.

Work of the load q: The work W_q produced by the load q acting on the free surface can be expressed by Equation (24) as a function of the radius $R_{\theta,\alpha=0}$ (Equation (15) and Figure 6) and of the velocity of the soil on the free surface $v_{\theta,\alpha=0}$.

$$W_q = \int_{R_{\theta=0,\alpha=0}}^{R_{\theta=\theta_f,\alpha=0}} q \cdot v_{\theta,\alpha=0} \cdot \mathrm{d}R_{\theta,\alpha=0} \tag{24}$$

Again, every point between E and C belongs to one logarithmic spiral described by the angle $\theta \in [0; \theta_f]$. The velocity of a point between E and C can be written as a function of θ, by means of Equation (5), with $\alpha=0$:

$$v_{\theta,\alpha=0} = v_\theta \cdot \mathrm{e}^{\tan\varphi \cdot (\alpha-\theta)} = v_\theta \cdot \mathrm{e}^{-\theta \cdot \tan\varphi} \tag{25}$$

The velocity $v_{\theta,\alpha=0}$ must, however, be expressed separately for *EB* and *BC*.

The line *EB* (described by $\theta \in [0; \theta_0]$) is subjected to a rotation around O with a rotational velocity Ω_E. The velocity of the soil against the upper part of the wall (*AE*) is then given by

$$v_\theta = \frac{v_{h0}}{x \cdot \tan\theta_0} \cdot \frac{x}{\cos\theta} = \frac{v_{h0}}{\tan\theta_0 \cdot \cos\theta} \tag{26}$$

Introducing Equation (26) in Equation (25), the velocity along *EB* becomes

$$v_{\theta,\alpha=0} = \frac{\mathrm{e}^{-\theta \cdot \tan\varphi}}{\tan\theta_0 \cdot \cos\theta} \cdot v_{h0} \quad \text{for } \theta \in [0; \theta_0] \tag{27}$$

The velocity along *BC* is obtained by introducing Equation (4) in Equation (25):

$$v_{\theta,\alpha=0} = \mathrm{e}^{-\theta \cdot \tan\varphi} \frac{\tan\theta_f - \tan\theta}{\tan\theta_f - \tan\theta_0} \cdot \frac{1}{\sin\theta} \cdot v_{h0} \quad \text{for } \theta \in [\theta_0; \theta_f] \tag{28}$$

As the centre O is aligned with the soil-free surface, the velocities calculated by Equations (27) and (28) are vertical.

The infinitesimal variation of $R_{\theta,\alpha=0}$ (Equation (15)), $\mathrm{d}R_{\theta,\alpha=0}$, can be expressed as a function of θ:

$$\frac{\mathrm{d}R_{\theta,\alpha=0}}{\mathrm{d}\theta} = \frac{x}{\cos\theta} \mathrm{e}^{-\theta \cdot \tan\varphi}(\tan\theta - \tan\varphi) \tag{29}$$

The work of the load W_q can thus be written as

$$W_q = W_{q,EB} + W_{q,BC} = \frac{q \cdot x \cdot v_{h0}}{\tan\theta_0} \int_0^{\theta_0} \cdot \frac{\tan\theta - \tan\varphi}{\cos^2(\theta)} \cdot \mathrm{e}^{-2\theta \cdot \tan\varphi} \cdot \mathrm{d}\theta$$

$$+ \frac{q \cdot x \cdot v_{h0}}{\tan\theta_f - \tan\theta_0} \int_{\theta_0}^{\theta_f} \frac{(\tan\theta_f - \tan\theta) \cdot (\tan\theta - \tan\varphi)}{\sin\theta \cdot \cos\theta} \cdot \mathrm{e}^{-2\theta \cdot \tan\varphi} \cdot \mathrm{d}\theta \tag{30}$$

The solution to the above integral can be obtained numerically. As it is a function of the two geometrical parameters, it can be expressed in the form

$$W_q = v_{h0} \cdot q \cdot \overline{W}_q = v_{h0} \cdot q \cdot g(\xi, x) \tag{31}$$

Sum of all contributions: The sum of the contributions given by Equations (23) and (31) gives the external work W_{ext} as a function of the two geometrical parameters ξ and x and of the

velocity v_{h0}:

$$W_{\text{ext}} = (\overline{W}_\gamma + q \cdot \overline{W}_q) \cdot v_{h0} = (f(\xi; x) + q \cdot g(\xi; x)) \cdot v_{h0} \tag{32}$$

The external work can be determined numerically for given x and ξ.

4.2.2. Internal work. The internal work, or energy dissipation, D corresponds to the sum of the contributions of the wall, the soil and their interface:

$$D = D_{\text{wall}} + D_{\text{soil}} + D_{\text{int}} \tag{33}$$

As the dissipation of energy in a Mohr–Coulomb soil without cohesion with an associated flow rule is zero [5] and as the interface is perfectly smooth, the energy is only dissipated in the three plastic hinges of the wall.

The internal work, conventionally negative, is given by

$$D = D_{\text{wall}} = -M_R \cdot [(1 + \eta_u) \cdot \Omega_E + (1 + \eta_l) \cdot \Omega_D]$$

$$= -M_R \cdot \frac{v_{h0} \cdot [1 + \eta_u + (\eta_l - \eta_u) \cdot \xi]}{\ell_h \cdot (\xi - \xi^2)} = -M_R \cdot \frac{v_{h0} \cdot [1 + \eta_u + (\eta_l - \eta_u) \cdot \xi]}{x \cdot \tan \theta_f \cdot (\xi - \xi^2)} \tag{34}$$

4.2.3. Equation of virtual works. Expressing that the sum of the internal (Equation (34)) and external (Equation (32)) works must be zero according to the principle of virtual works [7], the ultimate load q_R depends only on the two geometrical parameters:

$$W_{\text{ext}} + D = 0 \Rightarrow q_R = \frac{1}{\overline{W}_q} \cdot \left(\frac{[1 + \eta_u + (\eta_l - \eta_u) \cdot \xi] \cdot M_R}{x \cdot \tan \theta_f \cdot (\xi - \xi^2)} - \overline{W}_\gamma \right) = h(\xi; x) \tag{35}$$

The governing mechanism, defined as the lowest upper bound, must then be obtained by a procedure of optimization with respect to the two parameters x and ξ. Details on one possible procedure are given in [17].

5. RESULTS

Figure 7(b) shows how the so-computed upper bound to the ultimate load q_R varies as a function of the flexural strength M_R of the wall, expressed by dimensionless variables, for three soils characterized by different friction angles. Supports with flexural strength equal to the flexural of the wall ($\eta_u = \eta_l = 1$) and with no flexural strength ($\eta_u = \eta_l = 0$) are shown. The trends are in good agreement with the trends observed typically for any retaining structure, such as cantilever retaining walls: the ultimate load decreases as the friction angle of the soil decreases. The intersection of the curves with the x-axis indicates the flexural strength of the wall required to support the earth pressure due to the self weight of the soil ($q = 0$).

Figures 7(c) and 7(d) represent the geometrical parameters describing the mechanism leading to the lowest upper bound as a function of the friction angle of the soil and of the applied load. One interesting feature is that the position of the plastic hinge in the central zone of the wall, given by ξ, is almost independent of the friction angle of the soil, suggesting that the earth pressure distribution along the wall is hardly affected by this parameter. This plastic hinge is located at a distance of $0.58\ell_h$ from the top of the wall when no load is applied on the free surface. Its location becomes higher as the applied load increases.

Figure 7(e) presents a comparison between the solution based on the proposed mechanism, the solution obtained assuming the Rankine active earth pressure distribution along the wall [8] and the solution according to Terzaghi (averaged Rankine active earth pressure along the wall, [1]). According to the theory of plasticity [5–7], the solution based on the Rankine active earth pressure corresponds to a lower bound to the ultimate load since the stress field is statically admissible and does not violate the yield criterion anywhere in the soil. It clearly shows that the proposed
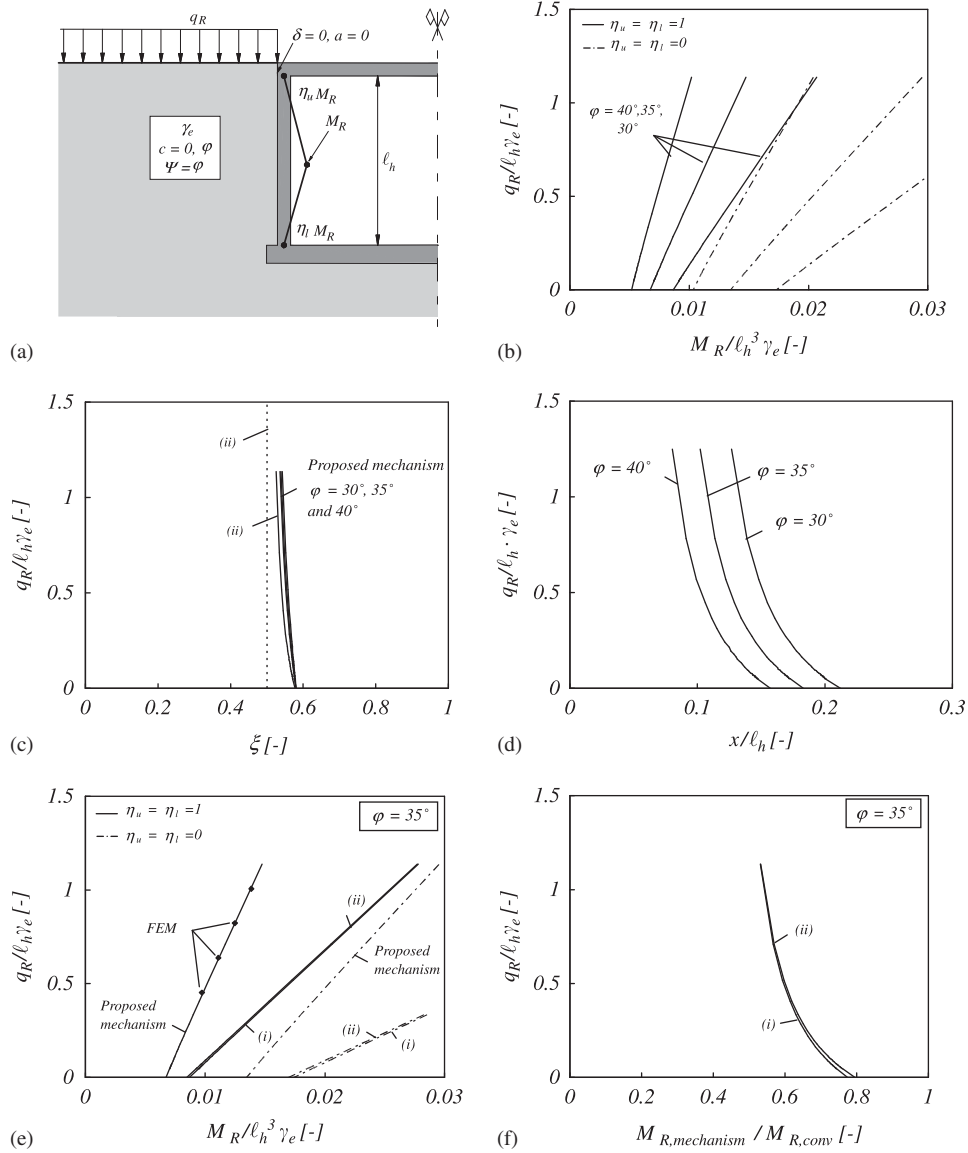
Figure 7. Lowest upper bound according to the proposed failure mechanism: (a) studied configuration; (b) ultimate load as a function of the flexural strength, support conditions and height of the wall, soil friction angle and soil unit weight; (c) position of the plastic hinge in the central region of the wall; (d) position of the centre O; (e) Comparison of the proposed solution with the solutions based on (i) Rankine active earth pressures [8], (ii) a constant averaged Rankine active earth pressure [1] and with results from the numerical modelling (see also Figure 10); and (f) Comparison of the required flexural strength of the wall for a given load according to the proposed solution and the conventional solutions (i) and (ii).

upper-bound solution is much more favourable than the conventional solutions. However, as the proposed solution is an upper bound, no theoretical conclusion can be drawn from this comparison. Nevertheless, as the failure mechanism corresponding to the Rankine active stress state in the soil is very different from the assumed failure mechanism of the wall, a non-negligible difference could be expected between the Rankine-based lower-bound solutions and the exact solution.

Figure 8 gives the geometry of the critical mechanism for two ultimate loads and for different friction angles of the soil. The observed tendency is again similar to that observed for other retaining structures. The amount of soil participating actively in the mechanism increases as the soil strength decreases. In this case, the applied load has also a similar influence.
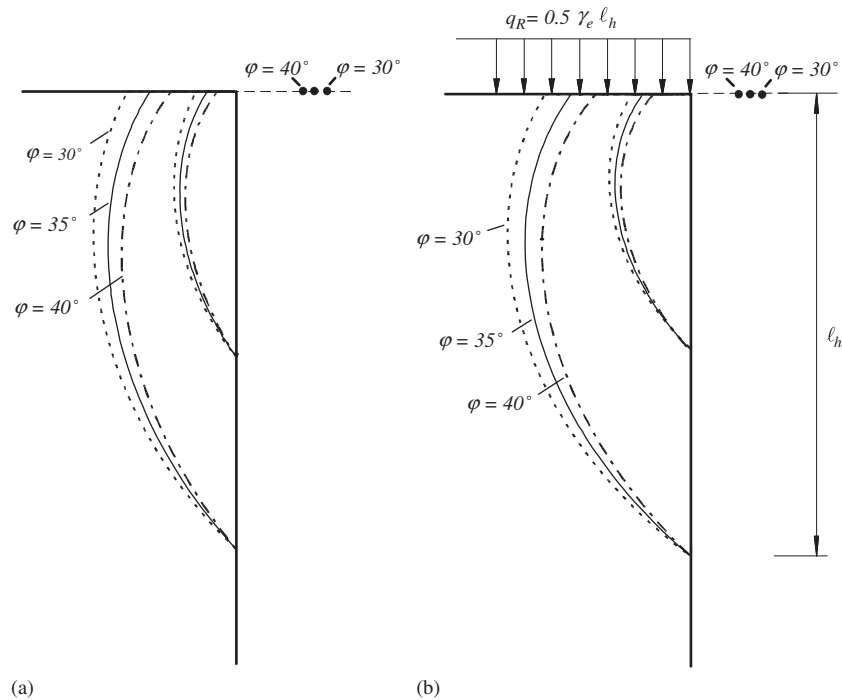
Figure 8. Influence of the soil friction angle on the critical failure mechanism (lowest upper bound):
(a) $q_R = 0$ and (b) $q_R = 0.5\gamma_e \cdot \lambda_h$.

6. COMPARISON WITH AN FEM MODEL

To evaluate the accuracy of the proposed solution, the same example is investigated using the FEM program Z-soil [18]. Its capacity to solve problems where plastic mechanisms are involved was tested successfully by the authors by evaluating the bearing capacity of a strip footing and comparing the numerical solutions with theoretical solutions [17].

The mesh used in the analysis is shown in Figure 9(a). The soil is modelled as an elastic perfectly plastic continuum with a Mohr–Coulomb yield criterion and an associative flow rule. A small cohesion is set to ensure numerical convergence. The wall is modelled by elasto-plastic-layered beam elements. The cross-section is divided into 10 layers, whose behaviour is given by a unidirectional elastic perfectly plastic law (see Figure 9(b)). This defines the cross-sectional behaviour of the beam. The flexural strength M_R is directly related to the yield stress of the material f_y defining the layers' behaviour. The soil and the wall are separated by contact elements that reproduce the behaviour of a perfectly smooth interface. Mesh-locking is solved suitably by the program.

For a given flexural strength of the wall, the applied load was incremented progressively by very small steps until the failure mechanism was completely developed (ultimate load). This condition was fulfilled when the strains increase rapidly between two load steps indicating that an asymptote, typical of the development of a plastic mechanism, was reached.

Figure 7(e) shows a comparison between the numerical model and the three previously discussed solutions. The numerical model is indeed in very good agreement with the proposed solution. As the FEM-calculation tends to the exact solution, this suggests that the proposed upper-bound solution is rather close to the exact solution. A corollary is that the conventional designs based on a Rankine active distribution [8] are very conservative. The additional capacity may be attributed to the development of unloading arches in the soil, as shown on Figure 10(b), which compares the earth pressure distribution calculated numerically with the other discussed solutions. A stress concentration is visible at the top of the wall, indicating that unloading arches are developing in the soil and
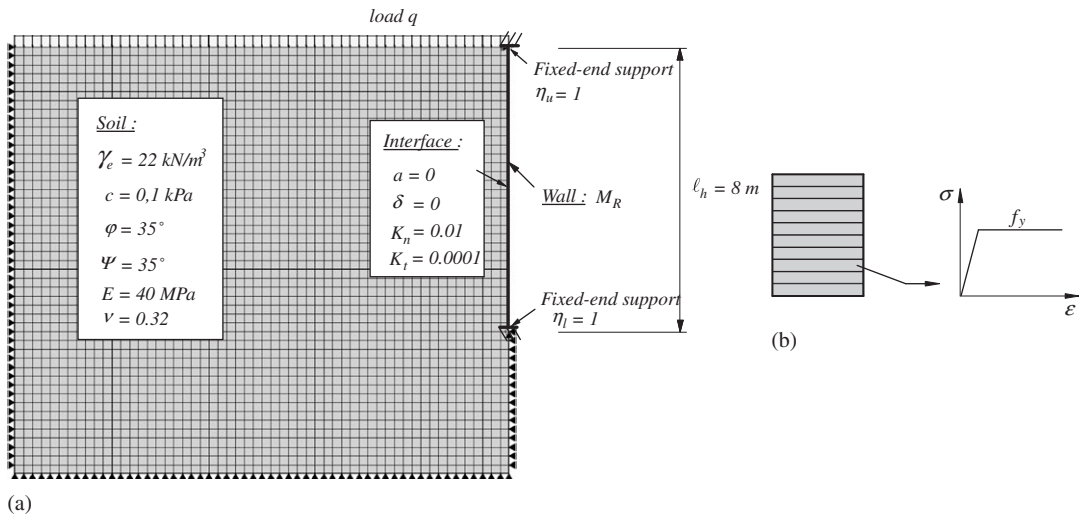
Figure 9. Finite element model: (a) geometry, supports and material properties and (b) beam element simulating the wall behaviour.
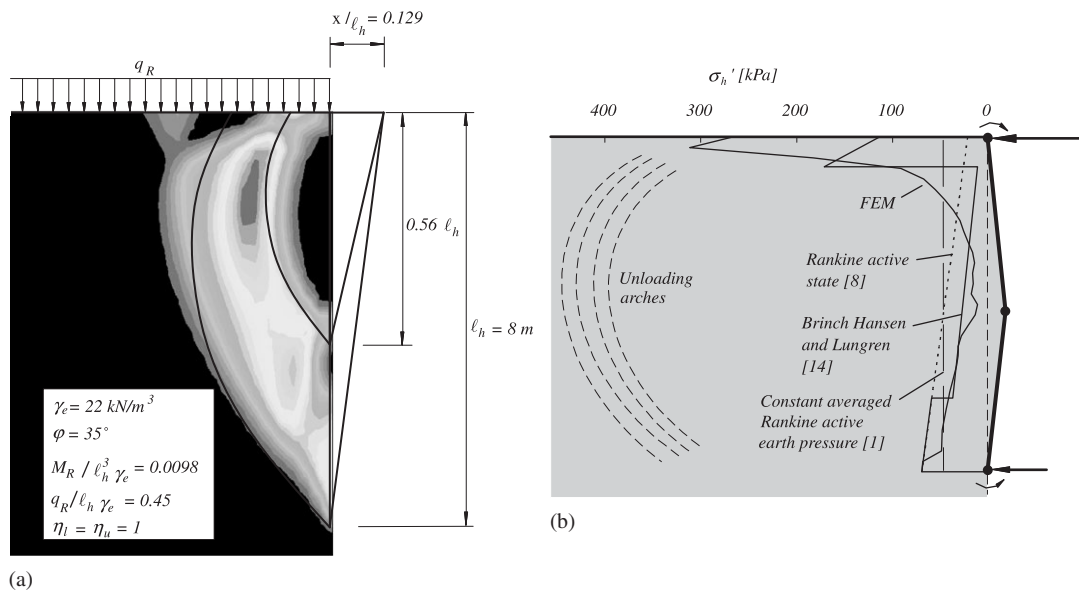

Figure 10. (a) Comparison of the proposed mechanism with an image of the failure mechanism according to the numerical model (increment of second invariant of the deformation $J_{2,\varepsilon}$) and (b) comparison of the numerically computed and theoretical earth pressure distributions for one example.

taking support on the top of the wall. The earth pressure in the central region of the wall is considerably reduced in comparison to the linear distribution. The figure also shows that for this given example, the earth pressure distribution obtained according to Brinch Hansen and Lundgren [14] is in good agreement with the numerical model. An important part of the earth pressure is indeed transmitted to the wall supports by the soil itself. These favourable phenomena can be attributed to the presence of a lateral support on top of the wall. This is indeed a consequence of the wall static system.

In practice, the stated problem is often posed differently. The wall strength must be chosen to resist a given load q. Figure 7(f) illustrates in this case the additional capacity available according to the proposed solution in comparison to the conventional solutions.

Figure 10(a) also indicates that the proposed mechanism reproduces well the numerically computed failure mechanism, which recalls some particularities of the trumpet zone described by Mortensen and Steenfelt [16].

7. CONCLUSIONS

The theory of plasticity was applied to a perfectly smooth braced retaining wall laterally supported at both ends, assuming that the wall fails in bending due to the development of three plastic hinges. An upper-bound solution was developed based on a kinematically admissible failure mechanism for soils with negligible cohesion, which considers a simultaneous failure of the soil and of the wall. The failure mechanism in the soil is composed of a rigid body and a plasticized (or shear) area delimited by logarithmic spirals. The proposed solution is found to be in very good agreement with the results from a finite element modelling. This suggests that it is indeed close to the exact solution. The stress state in the soil behind the wall and thus the earth pressure acting on the wall are found to be more favourable than the conventional stress states. This additional capacity is attributed to the development of arching effects in the soil between the wall supports, which have a positive influence on the bearing capacity of the wall.

NOMENCLATURE

A	area
D	energy dissipation
E	soil Young's modulus
$J_{2,\varepsilon}$	second invariant of the strain tensor
K	contact element stiffness
M_R	wall flexural strength
R	log spiral radius
W	work
a	interface adhesion
c	soil cohesion
f_y	yield strength
q	applied load on the free surface
v	velocity
x	position of the log spirals' pole
z	depth
ℓ_h	wall height
Ω	angular velocity
Ψ	soil dilatancy angle
α	angle
χ	curvature
δ	interface friction angle
ε	strain
γ	shear strain
γ_e	soil unit weight
φ	soil friction angle
v	Poisson ratio
σ	stress
θ	angle describing a log spiral
ξ	position of the central plastic hinge

REFERENCES

1. Terzaghi K, Peck RB. *Soil Mechanics in Engineering Practice* (2nd edn). Wiley: New York, 1967; 729.
2. Eurocode 7. Geotechnical design—part 1: general rules. *prEN 1997-1, Final Draft*, November 2004; 175.
3. Swiss Society of Civil Engineers and Architects. *SIA 267—Geotechnical Design*, Zürich, Switzerland, 2003.
4. Brinch Hansen J. Earth pressure calculation. *The Danish Technical Press*. The Institution of Danish Civil Engineers: Copenhagen, Denmark, 1953; 271.
5. Chen WF. *Limit Analysis and Soil Plasticity*. Elsevier: Amsterdam, 1975; 638.
6. Salençon J. An introduction to the yield design theory and its application to soil mechanics. *European Journal of Mechanics A/Solids* 1990; **9**:477–500.
7. Muttoni A, Schwartz J, Thürlimann B. *Design of Concrete Structures with Stress Fields*. Birkäuser: Basel, 1997.
8. Rankine WJM. On the stability of loose earth. *Philosophical Transactions of the Royal Society of London* 1857; **147**:9–27.
9. Vollenweider U, Pralong J. Analysis and design of cut-and-cover tunnels (In french: calcul et dimensionnement des tunnels exécutés à ciel ouvert). Office fédéral des routes, Suisse, 1998; 77.
10. Lambe WT, Whitman RV. *Soil Mechanics*. Wiley: New York, 1969; 553.
11. Lang GH-J, Huder J. *Bodenmechanik und Grundbau* (3rd edn). Springer: Berlin, Germany, 1985; 252.
12. Swiss Society of Civil Engineers and Architects. *SIA 261—Actions on Structures*, Zürich, Switzerland, 2003.
13. Meem JC. The bracing of trenches and tunnels. *Transactions of the American Society of Civil Engineers* 1908; **60**:1–23.
14. Brinch Hansen J, Lundgren H. *Hauptprobleme der Bodenmechanik*. Springer: Berlin, Germany, 1960; 282.
15. Steenfelt JS. Trumpet zone solution for line ruptures in undrained clay applied to the design of retaining walls. *Third International Conference on Numerical Methods in Geomechanics*, Aachen, Germany, 1979; 1193–1203.
16. Mortensen N, Steenfelt JS. Danish plastic design of sheet pile walls revisited in the light of FEM. *Proceedings of the Fifteenth International Conference on Soil Mechanics and Geotechnical Engineering*, Istanbul, Turkey, vol. 2, 2001; 1211–1218.
17. Plumey S. Soil–structure interaction in cut-and-cover tunnels (In french: interaction soil–structure dans le domaine des tranchées couvertes). *EPFL Ph.D. Thesis*, vol. 3714, Lausanne, Switzerland, January 2007; 299.
18. Zace Service SA. *Z.Soil.PC.2003 User's Manual*. Elmepress: Lausanne, Switzerland, 2003.